iScience

CellPress
OPEN ACCESS

Article

Changes in neuropeptide large dense core vesicle trafficking dynamics contribute to adaptive responses to a systemic homeostatic challenge

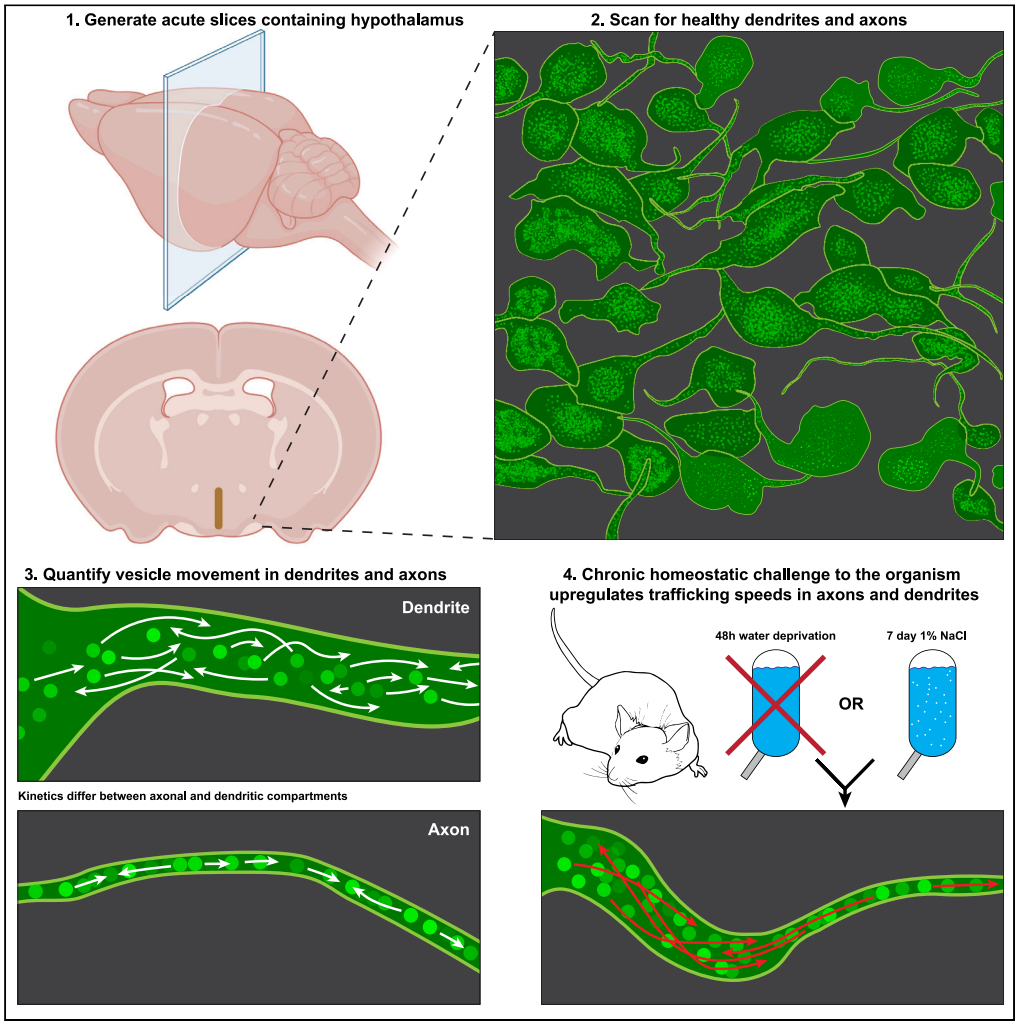

Matthew K. Kirchner, Ferdinand Althammer, Kevin J. Donaldson, Daniel N. Cox, Javier E. Stern

jstern@gsu.edu

Highlights

Quantification of LDCV dynamics in dendrites and axons of VP neurons

Different baseline VP-LDCVs trafficking dynamics between dendrites and axons

Acute changes in firing activity modestly altered VP-LDCVs trafficking dynamics

Chronic osmotic challenges upregulated LDCV trafficking in dendrites and axons

Kirchner et al., iScience 26, 108243
November 17, 2023
https://doi.org/10.1016/j.isci.2023.108243

iScience

CellPress
OPEN ACCESS

Article

Changes in neuropeptide large dense core vesicle trafficking dynamics contribute to adaptive responses to a systemic homeostatic challenge

Matthew K. Kirchner,[1,2] Ferdinand Althammer,[1,4] Kevin J. Donaldson,[2,3] Daniel N. Cox,[2,3] and Javier E. Stern[1,2,5,*]

SUMMARY

Neuropeptides are packed into large dense core vesicles (LDCVs) that are transported from the soma out into their processes. Limited information exists regarding mechanisms regulating LDCV trafficking, particularly during challenges to bodily homeostasis. Addressing this gap, we used 2-photon imaging in an *ex vivo* preparation to study LDCVs trafficking dynamics in vasopressin (VP) neurons, which traffic and release neuropeptide from their dendrites and axons. We report a dynamic bidirectional trafficking of VP-LDCVs with important differences in speed and directionality between axons and dendrites. Acute, short-lasting stimuli known to alter VP firing activity and axonal/dendritic release caused modest changes in VP-LDCVs trafficking dynamics. Conversely, chronic/sustained systemic osmotic challenges upregulated VP-LDCVs trafficking dynamic, with a larger effect in dendrites. These results support differential regulation of dendritic and axonal LDCV trafficking, and that changes in trafficking dynamics constitute a novel mechanism by which peptidergic neurons can efficiently adapt to conditions of increased hormonal demand.

INTRODUCTION

A fundamental property of all neurons is the vesicular release of neurotransmitter or neuropeptide via action potential-triggered exocytosis. These vesicles fall into two broad categories based on their appearance under electron microscopy: smaller clear core vesicles (CCVs), which are typically packaged with classic neurotransmitters such as glutamate or acetylcholine, and large dense core vesicles (LDCVs) which usually contain bigger molecules, particularly neuropeptides. Much of what is currently known about CNS neurotransmission, including neurotransmitter synthesis, packaging, factors regulating their release, and mechanisms modulating synaptic strengths, originated from studies limited to CCVs.[1,2] Neurotransmitter signals within CCVs are loaded into synaptic terminals by neurotransmitter-specific vesicular transporters (such as VGluT or VAchT).[3] In contrast, LDCVs bud off at the *trans*-golgi and thus do not require vesicular transporter proteins.[4] Thus, due to a lack of peptide reuptake machinery,[5] neuropeptides must constantly be generated, packaged, and trafficked from the nucleus to the releasing sites, constituting a critical process for the normal function of central neuropeptidergic neurons. Notably, however, and compared to CCVs, the fundamental processes regulating LDCV biology, including trafficking dynamics, activity-dependent release, and replenishment following sustained activation, remain largely understudied.

Oxytocin (OT) and vasopressin (VP) magnocellular neurosecretory cells (MNCs) located in the hypothalamic supraoptic (SON) and paraventricular (PVN) nuclei are considered classical examples of central neuropeptidergic neurons. These neurons' axons bundle and project ventrally through the median eminence into the posterior pituitary. In response to physiological challenges such as an increase in plasma osmolality or during lactation,[6–8] MNCs neuropeptide cargo is released into the systemic circulation in an action potential frequency- and pattern-dependent manner.[9–12]

In addition to axonal transport and release, LDCVs containing OT and VP are also transported to proximal and distal dendrites, from where neuropeptides are released intranuclearly, to mediate autocrine, paracrine, and hormonal actions.[13–15] Dendritic release of OT and VP is a well-established phenomenon,[13,14,16–19] demonstrated to play fundamental roles in helping coordinate and sustain the rhythmic activity of these neurons in response to physiological demand.[20,21] Notably, neuropeptide release from dendritic LDCVs can occur independently of axonal release,[19,22,23] and a growing body of evidence indicates that the mechanisms regulating dendritic release, including the necessity of action potentials,[24] the engagement of glutamate NMDA receptors (NMDARs),[19,24] and the process of priming,[18,22] differ significantly from those regulating axonal release.[25–27] While much of the work on dendritic release of OT and VP has focused on elucidating mechanisms

[1]Center for Neuroinflammation and Cardiometabolic Diseases, Georgia State University, Atlanta, GA 30303, USA
[2]Neuroscience Institute, Georgia State University, Atlanta, GA 30303, USA
[3]Center for Neuromics, Georgia State University, Atlanta, GA 30303, USA
[4]Institute of Human Genetics, Heidelberg University Hospital, 69120 Heidelberg, Germany
[5]Lead contact
*Correspondence: jstern@gsu.edu
https://doi.org/10.1016/j.isci.2023.108243

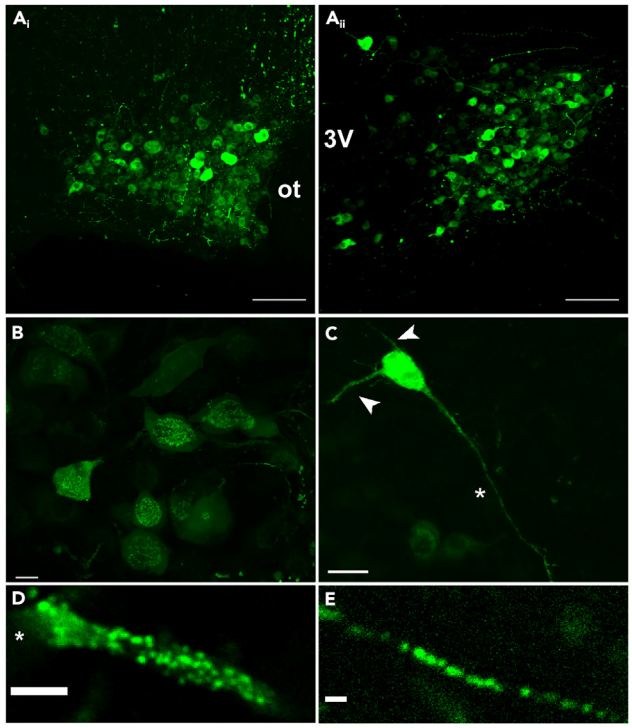

Figure 1. Representative examples of VP-containing LDCVs in various neuronal compartments of SON and PVN EGFP-VP neurons

(A) 2-photon images showing EGFP-VP neurons in the entire SON (*i*) and PVN (*ii*) at 20x magnification with optic tract (ot) and 3rd ventricle (3V) as landmarks for SON and PVN, respectively. Scale bars = 100 μm.

(B) Higher magnification image (40x) of the SON showing the distribution of EGFP-VP-LDCVs in the soma and processes. Scale bar = 10 μm.

(C) z stack projection of a single EGFP-VP neuron showing short dendrites without spines (arrows), contrasted with the narrow, long projecting axon (asterisk). Scale bar = 25 μm.

(D) A cropped VP dendrite containing LDCVs at 60x magnification, where movement could be tracked. Soma is cropped to the left (asterisk). Scale bar = 2 μm.

(E) A cropped VP axon containing LDCVs at 60x magnification, where movement could be tracked. Scale bar = 1 μm.

that regulate the process of exocytosis, little is known about those implicated in vesicular trafficking from the nucleus to the farthest reaches of MNC processes, including dendrites. This is functionally relevant for this system given that, as stated earlier, release of OT and VP into the bloodstream to mediate actions at peripheral targets prevents these neurons from recycling vesicle product at the synapse, resulting in constant demand for *de novo* peptide synthesis and trafficking.[28,29] Thus, MNCs constitute an ideal central neuropeptidergic model to study precise mechanisms regulating LDCV trafficking dynamics, particularly within dendritic compartments.

In this study, we performed high-resolution 2 photon imaging in hypothalamic slices obtained from a transgenic rat expressing EGFP tethered to the C-terminal of VP.[30] Thus, in this rat model EGFP is fused directly to VP and stored within the LDCVs, enabling visualization of LDCV in both axonal and dendritic processes. Using this approach, we quantitatively assessed for the first time LDCV trafficking properties in axons and dendrites of VP MNCs under basal conditions, in response to acute changes in neuronal activity, and following systemic physiological challenges that imposed a chronic and sustained demand for VP activity and neuropeptide release.

RESULTS

Basal characteristics of VP-LDCV trafficking properties

LDCVs containing EGFP-VP were observed as fluorescent spherical puncta in all SON and PVN neuronal compartments including soma, axons, and dendrites (Figure 1A, Video S1). A total number of 11,505 LDCVs in 68 processes from 37 rats were analyzed in this study. In somata, pools of LDCVs were visualized clustered around nuclei and, for the most part, they were inert (Figure 1B). LDCVs were readily observed in processes, and their density varied highly between neurons (Figures 1C–1E). Compared to somata, LDCVs in axons and dendrites were often very active, moving bidirectionally in an anterograde and retrograde manner.

To quantitatively assess LDCVs movement, we targeted process segments visible in a single z-plane with a minimum length of 15 μm, containing a high density of LDCVs (Figure 2A, Video S2). LDCVs had an average puncta diameter of 0.34 ± 0.004 μm (Figure 2B). No differences were observed in the size of dendritic compared to axonal LDCVs. In both cases, LDCVs were found to travel both anterogradely and retrogradely, with the proportion of anterograde:retrograde movement directionality being significantly higher in axons compared to dendrites

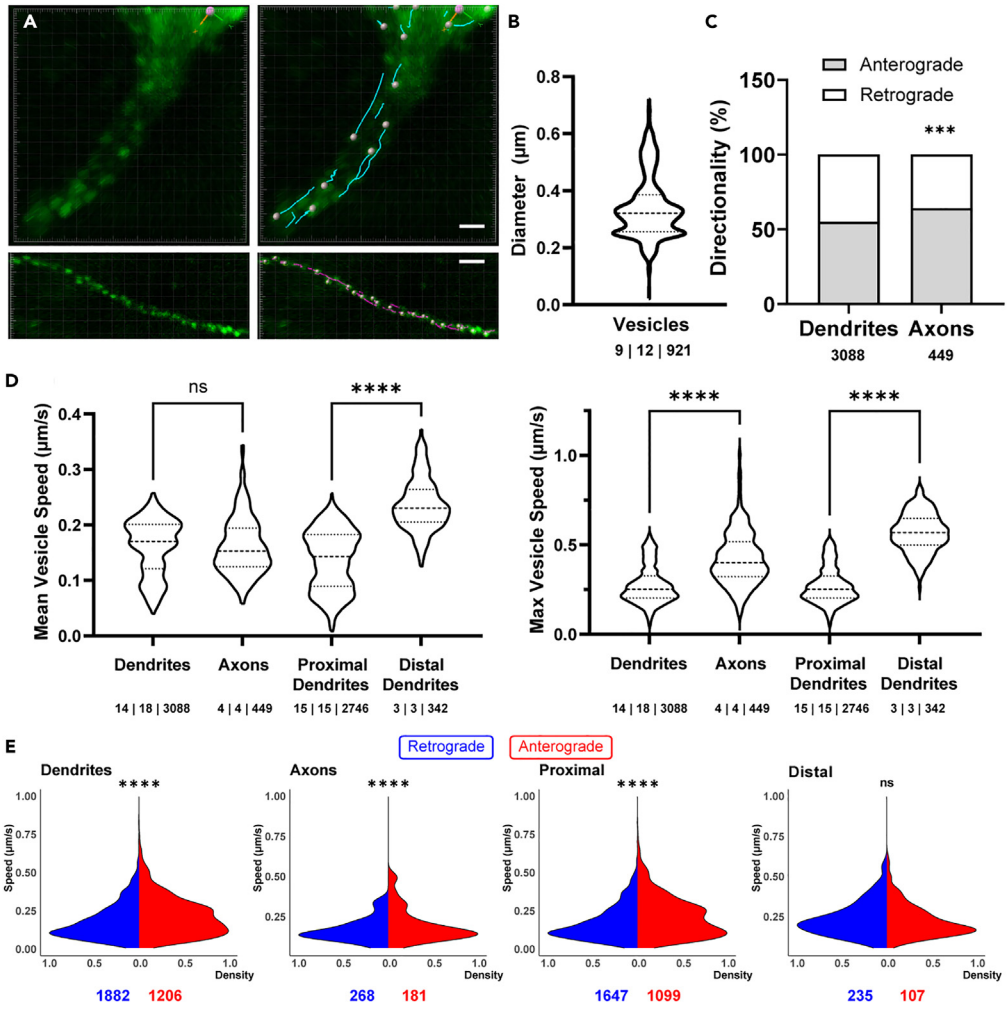

Figure 2. Characterization of VP-LDCVs trafficking properties under basal conditions

(A) Single-frame image from a 2-photon time series capture of VP-LDCV movement in an apical dendrite (*top*) and an axon (*bottom*) of a VP neuron, showing both the raw image (*left*) and the Imaris analysis overlay (*right*). Scale bars: 2 µm.

(B) Violin plot showing the mean VP-LDCV diameter.

(C) Summary of directionality of all tracked LDCVs under baseline conditions. The incidence of LDCVs traveling anterogradely in axons is statistically higher than that in dendrites (***$p < 0.003$, chi-squared test). Numbers below each group represent n values (LDCVs).

(D) Violin plots of mean (left) and max (right) speeds of VP-LDCVs. ****$p < 0.0001$, one way ANOVA, Šidák multiple comparisons test.

(E) Mean speed density distribution of VP-LDCVs traveling in retrograde and anterograde direction. Numbers below each group represent n values (LDCVs).

(Figure 2C; 64.2% ± 3.4% [n = 5 processes] and 55% ± 0.7% anterograde [n = 18 processes] for axons and dendrites, respectively, $p < 0.001$). The mean basal speed of LDCVs movement in all processes was 0.19 ± 0.001 µm/s, with a mean max speed of 0.37 ± 0.004 µm/s. In many cases, however, we observed LDCVs traveling at 1–1.5 µm/s. A detailed quantification of LDCVs movement under basal conditions for the pooled LDCV data, as well as a breakdown based on morphological compartment (in axons vs. dendrites), and proximity to soma along the dendrite (proximal dendrites [<15 µm from soma] vs. distal dendrites [>50 µm from soma]), is presented in Figure 2 and summarized in Table 1. While we observed no difference in the mean speed between dendrites and axons ($p > 0.05$), the max LDCV speed was slower in the former ($p < 0.0001$). Notably, LDCVs traveled significantly faster in distal when compared to proximal dendritic segments ($p < 0.0001$ for both mean and max speed) (Figure 2D).

In addition to overall speed of movement, we also compared the distribution of LDCV mean speed traveling anterogradely versus retrogradely (Figure 2E). The distribution of LDCVs traveling anterograde versus retrograde was statistically significant in all comparisons except for trafficking in distal dendrites (dendrites $p < 0.0001$; axons $p < 0.0001$; proximal dendrites $p < 0.0001$; distal dendrites $p > 0.05$). The mean speed of LDCVs traveling anterograde compared to retrograde was faster in dendrites ($p < 0.0001$), while it was significantly slower in axons ($p < 0.0001$). When examining a breakdown of proximal and distal dendrites, proximal dendrites showed faster anterograde speeds

Table 1. Basal properties of LDCV speeds

Group	Dendrites	Axons	Proximal Dendrites	Distal Dendrites
n	14 | 18 | 3088	4 | 4 | 449	11 | 15 | 2746	3 | 3 | 342
Mean Speed (μm/s)	0.19 ± 0.001	0.16 ± 0.004	0.20 ± 0.002	0.23 ± 0.004
Max Speed (μm/s)	0.37 ± 0.004	0.42 ± 0.012	0.35 ± 0.004	0.56 ± 0.011

compared to retrograde ($p < 0.0001$) while there was no difference in mean directionality speed in distal dendrites (see Table 2 for full anterograde vs. retrograde breakdown).

Kinetics of dendritic LDCV replenishment

Next, we evaluated the kinetics of dendritic LDCV replenishment. To this end, we used fluorescence recovery after photobleaching (FRAP). Namely, we photobleached dendritic compartments for 30 s and then measured the rate of LDCV recovery over time (Figures 3A and 3B). We plotted LDCV spots/frame as normalized to baseline measurements (Figure 3C). The resulting curve could be confidently fit with a double exponential (fast component: $\tau = 1.89 \pm 0.2$ s; amplitude = 0.41 ± 0.03; slow component $\tau = 77.2 \pm 70.9$ s; amplitude = 1.2 ± 0.8). This indicates that dendritic LDCV replenishment occurs relatively rapidly, and that the observed trafficking activity reflected newly trafficked LDCVs, rather than same LDCVs "patrolling" back and forth along the longitudinal axis of the dendrite.

Is basal LDCV trafficking regulated in an activity-dependent manner?

To determine to what extent LDCV trafficking in dendrites is dependent on the basal activity levels of VP neurons, we examined firsts whether silencing the neurons would affect trafficking dynamics. As shown in Figure 4A (see also Table 3), we found than bath application of TTX (1 μM) induced no significant changes in mean speed ($p > 0.05$). Conversely, the max speed decreased significantly ($p < 0.0001$). Additionally, trafficking directionality (i.e., % anterograde travel) was not significant after TTX application ($p > 0.05$, n = 8 processes).

We next examined whether an acute increase in VP neuronal activity known to evoke dendritic release of VP affected LDCV trafficking properties. Glutamate is a key excitatory transmitter in SON neurons, and activation of both synaptic and extrasynaptic NMDARs has been shown to promote spiking activity and evoke dendritic release of VP.[19,24,31,32] We therefore evaluated the effects of an acute NMDA application on LDCV trafficking properties. We found that bath application of NMDA (10 μM, 3–5 min) upregulated mean trafficking speed ($p < 0.0001$) and max speed ($p < 0.0001$), without affecting trafficking directionality ($p > 0.05$, n = 9 processes) (Figure 4B; Table 3.)

VP neuronal activity and dendritic release of VP can also be stimulated and triggered by an acute osmotic stimulation.[33,34] We therefore tested whether a local osmotic challenge affected trafficking dynamics. We used a +20 mOsm challenge as it is physiologically relevant for VP secretion and has been previously shown to increase VP release *ex vivo*.[24,33] We found that increasing ACSF osmolality from 301 ± 2 to 320 ± 3 mOsm (mannitol 0.2%, 3–5 min) failed to significantly alter LDCV trafficking mean speed, max speed, or directionality ($p > 0.05$, n = 5 processes) (Figures 4C; Table 3).

Chronic stimulation of VP neurons and their effect on LDCV trafficking properties

In addition to acute stimuli known to trigger exocytosis of readily releasable pools of VP-LDCVs, MNCs are plastic neurons whose activity changes in response to systemic whole-body homeostatic challenges like dehydration and salt loading (SL).[35–38] Acute stimuli reported earlier

Table 2. Basal speeds of anterograde and retrograde vesicles

	Anterograde	*n*	Retrograde	*n*	unpaired t test (Ant vs. Ret)
Dendrites					
Mean	0.20 ± 0.003	1882	0.1839 ± 0.003	1206	****p < 0.0001
Max	0.35 ± 0.009		0.44 ± 0.01		****p < 0.0001
Axons					
Mean	0.14 ± 0.005	268	0.20 ± 0.007	181	****p < 0.0001
Max	0.45 ± 0.01		0.36 ± 0.01		*p < 0.05
Proximal Dendrites					
Mean	0.22 ± 0.003	1647	0.18 ± 0.003	1099	****p < 0.0001
Max	0.35 ± 0.01		0.42 ± 0.01		****p < 0.0001
Distal Dendrites					
Mean	0.24 ± 0.007	235	0.26 ± 0.01	107	p > 0.05
Max	0.55 ± 0.01		0.59 ± 0.02		p > 0.05

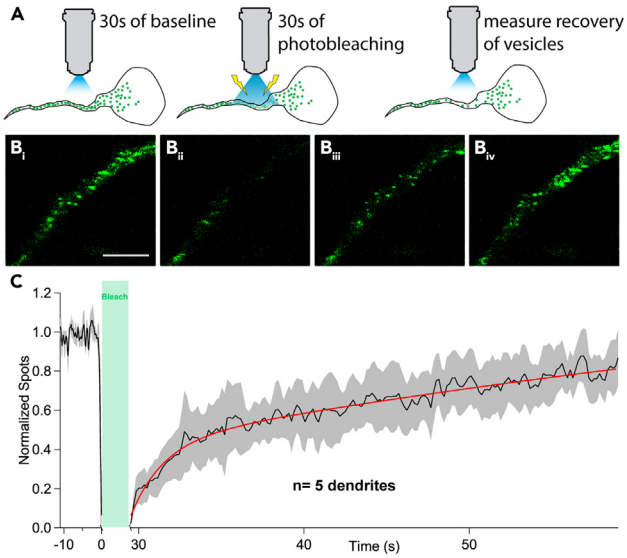

Figure 3. VP-LDCV trafficking kinetics following fluorescence recovery after photobleaching (FRAP)

(A) Diagrammatic depiction of protocol used for FRAP.

(B) Image of a dendrite undergoing the FRAP protocol showing baseline prior to photobleaching (*i*), immediately after photobleaching (*ii*), 15 s after photobleaching (*iii*), and 60 s after photobleaching (*iv*), when LDCV recovery has plateaued. Scale bar = 5 μm.

(C) Plot of mean spots/frame normalized to the average of the baseline (n = 5 dendrites). The recovery curve was confidently fit to a double exponential (red line, τ_{fast} = 1.89 ± 0.2s and τ_{slow} = 77.2 ± 70.9s).

had a detectable yet modest effects on the trafficking properties of VP neurons; we therefore hypothesized that peptide trafficking could be more robustly altered in response to long-term homeostatic challenges to the VP system.

We tested two discrete prolonged osmotic homeostatic challenges to VP MNCs: A 48-h water deprivation (WD) and a 7-day SL regiment wherein normal drinking water was replaced with water containing 1% NaCl. These are widely used models for studying the effects of chronic osmotic challenge[39–41] on the upregulation of VP synthesis and release,[30,42–44] as well as on the downstream consequences on whole animal physiology.[45–47] Under both WD and SL challenges, the mean and max trafficking speeds increased significantly and robustly relative to controls ($p < 0.0001$ in both cases Figures 5A and 5B, Video S3), in both dendrites and axons, demonstrating increases in speed between 42.6% and 131.1% (Table 4). Notably, in dendrites (but not axons), SL evoked a more robust effect in both mean and max LDCV speed when compared to WD ($p < 0.001$ for both parameters, Figures 5A and 5B). Furthermore, SL (but not WD) significantly increased the percentage of anterograde LDCV travel in dendrites ($p < 0.05$) but not in axons ($p > 0.05$) (Figure 5C).

Finally, we plotted kernel density functions of anterograde and retrograde movement in the three experimental conditions (control, WD, and SL) to evaluate the distribution of LDCV speeds. As shown in Figure 5D, the plots indicate that the LDCV mean speed distribution was significantly different between anterograde and retrograde travel in control ($p < 0.0001$), WD ($p < 0.01$), and SL ($p < 0.0001$) cases, supporting a higher speed in the anterograde direction. A full breakdown of mean and max speeds comparing anterograde and retrograde movement is in Table 5.

DISCUSSION

In this study, we employed high-resolution 2-photon imaging in a transgenic EGFP-VP rat to characterize dynamic trafficking of LDCVs in axons and dendrites of VP MNCs under basal conditions, as well as in response to acute and chronic challenges known to increase VP firing activity and to evoke both systemic and dendritic release of VP. To the best of our knowledge, this constitutes the first study to monitor trafficking dynamics of LDCV in VP neurons in real time, addressing adaptive changes in their dynamics in response to conditions of enhanced hormonal demand.

Highly dynamic trafficking of VP-LDCVs in axons and dendrites under basal conditions

Our approach allowed us to readily identify VP-containing LDCVs in dendrites and axons of VP MNCs and quantitatively assess velocity and directionality of their trafficking in these different neuronal compartments. We found that VP-LDCVs in both axons and dendrites displayed rapid movements in both anterograde and retrograde directions. Notably, we found important differences in directionality and velocity between axons and dendrites, as well as different dendritic segments (i.e., proximal vs. distal). For example, the max velocity was slower in dendrites compared to axons, whereas both the mean and max trafficking velocities were faster in distal compared to proximal dendritic

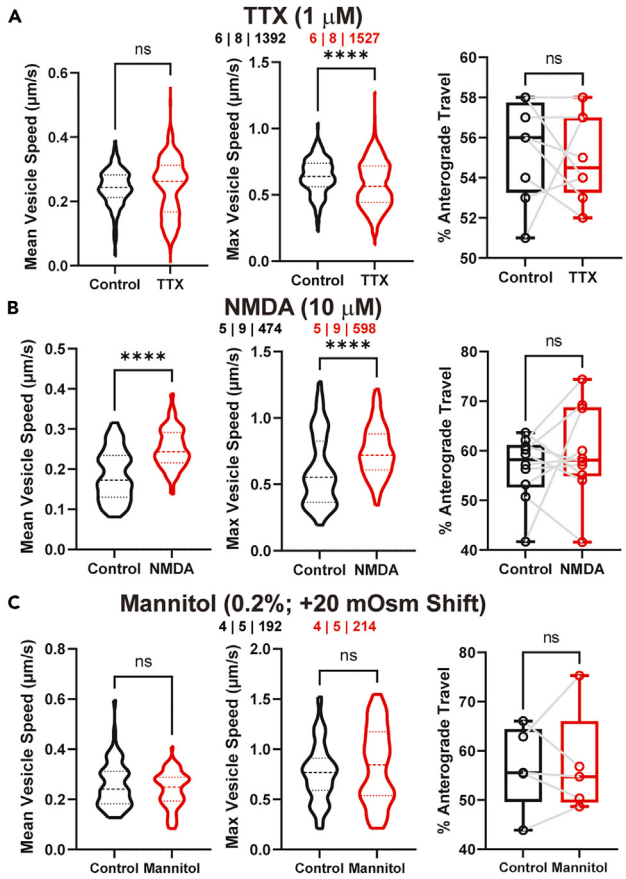

Figure 4. Changes in VP-LDCV trafficking dynamics in response to acute changes in VP neuronal activity

(A–C) Plots of dendritic LDCV mean speed (left), max speed (middle), and incidence of anterograde travel (right) under basal conditions and in response to (A) TTX (1 μM), (B) NMDA (10 μM), and (C) Mannitol (0.2%). Numbers at the top center of each panel represent n values (animals | dendrites | LDCVs). %Anterograde travel individual points represent 1 process. ****p < 0.0001, unpaired t test (Mean and Max vesicle speed), paired t test (%Anterograde Travel).

segments. In dendrites, anterograde trafficking displayed faster velocities compared to retrograde trafficking whereas the opposite was true for axons. Distal dendrites anterograde vs. retrograde speeds were statistically insignificant.

Trafficking of LDCVs in dendrites did not display a directionality preference, with approximately half traveling in the anterograde and the other half in retrograde directions. While anterograde traveling was significantly higher in axons, the percentage of those traveling retrogradely was still high (~35%) compared to other neuronal types.[48–50] While we currently lack an explanation for this, we need to consider

Table 3. Speeds of LDCVs affected by acute challenges in dendrites

Group	Control	TTX	%Δ	p values
n	6 | 8 | 1392	6 | 8 | 1527		
Mean Speed (μm/s)	0.24 ± 0.003	0.24 ± 0.002	0.50%	p > 0.05
Max Speed (μm/s)	0.63 ± 0.003	0.57 ± 0.007	−9.60%	****p < 0.0001
	Control	NMDA	%Δ	p values
n	5 | 9 | 474	5 | 9 | 598		
Mean Speed (μm/s)	0.18 ± 0.01	0.25 ± 0.004	38.90%	****p < 0.0001
Max Speed (μm/s)	0.60 ± 0.03	0.75 ± 0.02	25.00%	****p < 0.0001
	Control	Mannitol	%Δ	p values
n	4 | 5 | 192	4 | 5 | 214		
Mean Speed (μm/s)	0.26 ± 0.01	0.24 ± 0.01	−7.70%	p > 0.05
Max Speed (μm/s)	0.76 ± 0.04	0.83 ± 0.05	9.21%	p > 0.05

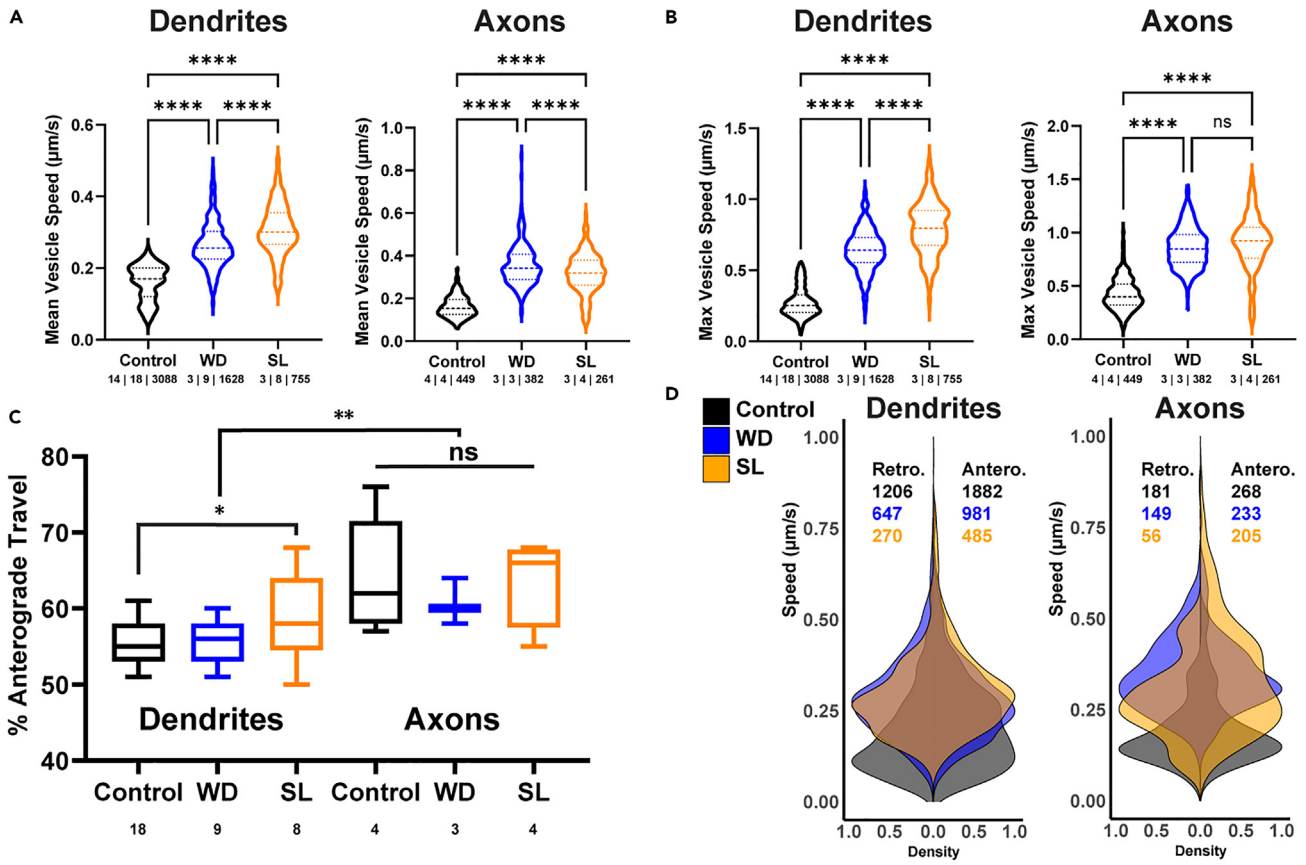

Figure 5. Changes in VP-LDCV trafficking dynamics in response to chronic osmotic challenges

(A) Violin plots of mean LDCV speed in dendrites (*left*) and axons (*right*) under euhydrated control conditions, 48 h of water deprivation (WD), and 7 days salt loading (SL). ***p < 0.0001, One Way ANOVA, Šidák multiple comparisons test.

(B) Violin plots of max LDCV speed in dendrites (*left*) and axons (*right*) under euhydrated control conditions, 48 h of water deprivation (WD), and 7 days salt loading (SL). Max LDCV speed of dendrites (*left*) and axons (*right*) compared under control conditions, WD, and SL. ***p < 0.0001, One Way ANOVA, Šidák multiple comparisons test.

(C) Summary of directionality of all tracked LDCVs under control euhydrated conditions, WD, and SL in dendrites and axons (**p < 0.01, two-way ANOVA). The only within-groups difference was between control and SL dendrites (*p < 0.05, Šidák multiple comparisons test). Numbers below each group represent n values (processes).

(D) Kernel density distributions of mean speed of VP-LDCV anterograde vs. retrograde traveling in control euhydrated, WD, and SL conditions from dendrites (*left*) and axons (*right*). Numbers in each plot represent n values, color coded to correspond to experimental group (LDCVs).

that, in the slice preparation, axons are cut off from their terminals at the posterior pituitary; thus, vesicles simply may switch direction when reaching a dead end.[51] Nonetheless, retrograde traveling has also been reported in intact axons both *in vivo* and cell culture conditions.[48,50,52]

The continuous abundant trafficking of LDCVs in VP MNCs stands as a possible mechanism by which neurons ensure resupply of neuropeptide to active sites of release, both at axonal terminals and dendrites. In addition to classical axonal release of VP into the peripheral circulatory system, VP neurons also release their LDCV cargo content from somatodendritic compartments, playing an important role in intrahypothalamic communication. Multiple studies demonstrate these diverse modes of release can be regulated independently and subserve different functional roles.[13,15,17,24] Still, whether compartment-specific differences in cargo trafficking properties, and/or their modulation by physiologically relevant challenges, existed in VP neurons remained until now unknown. Thus, in this context, our reported differences in LDCV trafficking behavior between dendrites and axons further support the importance of compartment-specific regulation of neuropeptide dynamics in VP MNCs.

A similar highly dynamic bidirectional trafficking of LDCVs was previously shown in other neuronal types (e.g., Neuropeptide Y LDCVs), both in cell cultures and *in vivo*.[48,50,52] This likely represents the presence of microtubules with mixed polarity[53] and an assortment of motor proteins in the processes of VP neurons traveling at various speeds.

Compared to previous reports in other neurons, the trafficking speeds reported in our studies were slower, but still within the range previously reported (from 0.7 to 1.5 µm/s).[48,51,52,54,55] Several factors could contribute to these differences in basal velocities. Firstly, almost all previous studies were performed either in cell cultures[54,55] or *in vivo* in mice[52] or drosophila.[51] Thus, it is possible that trafficking kinetics are

Table 4. Basal speeds of LDCVs affected by chronic challenges in dendrites and axons

	Dendrites				Axons			
	n	Mean speed (μm/s)	%Δ	p value	*n*	Mean speed (μm/s)	%Δ	p value
Control	14 | 18 | 3088	0.188 ± 0.001	–		4 | 4 | 449	0.164 ± 0.004	–	
WD	3 | 9 | 1628	0.29 ± 0.003	54.2%	****p < 0.0001	3 | 3 | 382	0.34 ± 0.005	111.6%	****p < 0.0001
SL	3 | 8 | 755	0.323 ± 0.005	71.8%	****p < 0.0001	3 | 4 | 261	0.33 ± 0.009	107.3%	****p < 0.0001
WD:SL %Δ	–	–	11.4%	****p < 0.0001	–	–	−2.0%	****p < 0.0001
		Max speed (μm/s)	%Δ			Max speed (μm/s)	%Δ	
Control		0.367 ± 0.004	–			0.424 ± 0.004	–	
WD		0.72 ± 0.006	96.2%	****p < 0.0001		0.861 ± 0.01	103.1%	****p < 0.0001
SL		0.848 ± 0.01	131.1%	****p < 0.0001		0.9369 ± 0.03	121.0%	****p < 0.0001
WD:SL %Δ	–	–	17.8%	****p < 0.0001	–	–	8.8%	p > 0.05

different in an acute slice preparation, even though our recordings were obtained close to physiological temperatures. This limitation should be acknowledged, as temperature is a factor that critically affects various processes' kinetics. Nonetheless, the slice offers the advantage of spatiotemporal resolution, stable imaging, and a paradigm in which much of the other work in VP neuron physiology can be more directly compared to. Particularly, it is an approach that retains *ex vivo* adaptive remodeling of the system (synaptic plasticity, firing properties, ion channel function, etc.) in response to *in vivo* challenges (e.g., chronic osmotic stimulation, lactation, pregnancy).[24,56–61] Another important difference is that we found LDCVs in VP neurons to be larger (~300 nm) compared to those previously reported in similar studies.[52,62,63] Still, whether larger LDCVs may also contribute to slower speeds is currently unknown. Lastly, LDCVs in VP neurons are densely packed and ubiquitous, as they are the primary vesicle product of these neurons, containing approximately 85,000 molecules/vesicle of the VP peptide.[26,64] This contrasts with cortical or CA1 pyramidal neurons which primarily package and release smaller CCVs containing glutamate.[65] Thus, the larger size and higher density of LDCVs may also contribute to the lower LDCV speeds observed in VP MNCs.

Finally, we wanted to address to what extent the basal velocity and/or directionality of VP-LDCV trafficking was activity dependent. We found that blocking action potential firing with TTX did not affect directionality and only slightly (though significantly, ~10%) diminished the max speed of travel. This would suggest that the basal dynamics of LDCVs trafficking in VP neurons are largely independent of the basal degree of VP neuronal activity. This observation aligns with previous studies showing that dendritic release can occur independently of action potentials.[23,24,66] In addition, it is possible that the lack of TTX effect may reflect a low level of basal activity of VP neurons in the slice preparation compared to *in vivo*.

We acknowledge that in some cases, as previously reported in other cells,[51,52] we observed LDCVs that would change direction or freeze mid-trajectory, which were not included in our analysis. Given, however, the large volume of vesicles analyzed, excluding these likely had a minor impact on the overall data reported. Nonetheless, this further supports the complexity and dynamic nature of LDCV trafficking in VP neurons.

VP-LDCVs speeds are scarcely modulated by acute, transient increases in firing activity but accelerate under chronic sustained challenges such as WD and SL

A critical question regarding LDCV trafficking in general is whether and how this phenomenon is regulated. In the case of VP neurons, we wanted to specifically address whether conditions and mechanisms that increase VP neuronal activity and dendritic/axonal release of the neuropeptide are accompanied by changes in VP-LDCV dynamics. Transient activation of glutamate NMDARs and an acute hyperosmotic stimulation are both known to increase the firing activity of VP neurons.[31,35,36,67–69] However, we recently showed that NMDAR-evoked firing, even for the same number or frequency of action potentials, evoked a much more robust dendritic release of VP.[24] In line with these previous findings, we report here that bath-applied NMDA significantly increased dendritic VP-LDCV mean and max trafficking velocities (~40% and ~25%, respectively, $p < 0.001$). Conversely, an acute increase of 20 mOsm in the ACSF (mannitol 0.2%), an approach previously shown to increase VP firing activity,[34,68] as well as dendritic release of VP[19,24] in the slice preparation failed to affect VP-LDCV velocities. Neither NMDA nor mannitol affected VP-LDCV trafficking directionality. Thus, these results suggest that an acute increase in the demands for dendritic release of VP could be sufficient to engage changes in dendritic VP-LDCV trafficking. To further explore this, rats were subjected to two discrete prolonged osmotic demands for VP hormone release, namely a 48 h WD and 7 days of 1% SL. Both these challenges are well characterized, and while both lead to an increase in plasma osmolality and VP synthesis and release,[70–72] SL has been reported to induce more pronounced changes in these parameters, compared to WD.[46] Moreover, it is important to highlight that numerous previous studies have shown that adaptive remodeling of the system in response to *in vivo* challenges (e.g., chronic osmotic stimulation, lactation, pregnancy) is still reflected in the *ex vivo* slice preparation (e.g., synaptic plasticity, firing properties, intrinsic properties, ion channel functioning, etc.),[24,56–61] further supporting that the slice preparation, despite its limitations (like any other approach) is an efficient model to study adaptive changes in the magnocellular system in response to systemic physiological changes. We found that VP-LDCV trafficking robustly

Table 5. Speeds of anterograde and retrograde vesicles affected by chronic challenges

	n	Anterograde (mm/s)	*n*	Retrograde (mm/s)	p values (Ant vs. Ret)	p values (Between groups)	
Dendrites (Mean Speed)							
Control	1882	0.20 ± 0.003	1206	0.1839 ± 0.003	****p < 0.0001	C v. WD Antero:	****p < 0.0001
WD	981	0.29 ± 0.004	647	0.29 ± 0.004	p > 0.05	C v. SD Antero:	****p < 0.0001
SL	485	0.32 ± 0.006	270	0.27 ± 0.006	****p < 0.0001	WD v. SD Antero:	****p < 0.0001
						C v. WD Retro:	****p < 0.0001
						C v. SD Retro:	****p < 0.0001
						WD v. SD Retro:	p > 0.05
Dendrites (Max Speed)							
Control	1882	0.35 ± 0.009	1206	0.44 ± 0.01	****p < 0.0001	C v. WD Antero:	****p < 0.0001
WD	981	0.73 ± 0.009	647	0.71 ± 0.01	p > 0.05	C v. SD Antero:	****p < 0.0001
SL	485	0.80 ± 0.01	270	0.83 ± 0.02	p > 0.05	WD v. SD Antero:	****p < 0.0001
						C v. WD Retro:	****p < 0.0001
						C v. SD Retro:	****p < 0.0001
						WD v. SD Retro:	****p < 0.0001
Axons (Mean Speed)							
Control	268	0.14 ± 0.005	181	0.20 ± 0.007	****p < 0.0001	C v. WD Antero:	****p < 0.0001
WD	233	0.35 ± 0.007	149	0.35 ± 0.008	p > 0.05	C v. SD Antero:	****p < 0.0001
SL	205	0.35 ± 0.01	56	0.27 ± 0.01	***p < 0.001	WD v. SD Antero:	p > 0.05
						C v. WD Retro:	****p < 0.0001
						C v. SD Retro:	****p < 0.0001
						WD v. SD Retro:	p > 0.05
Axons (Max Speed)							
Control	268	0.45 ± 0.01	181	0.36 ± 0.01	*p < 0.05	C v. WD Antero:	****p < 0.0001
WD	233	0.86 ± 0.01	149	0.87 ± 0.02	p > 0.05	C v. SD Antero:	****p < 0.0001
SL	205	0.98 ± 0.03	56	0.78 ± 0.04	**p < 0.01	WD v. SD Antero:	****p < 0.0001
						C v. WD Retro:	****p < 0.0001
						C v. SD Retro:	****p < 0.0001
						WD v. SD Retro:	p > 0.05

upregulated under these prolonged osmotic challenges, and that in dendrites (but not axons) larger effects were observed in SL compared to WD rats. Thus, we found both the mean and max dendritic and axonal speeds to be significantly increased in WD and SL, but only in dendrites did SL evoke significantly larger effects than WD. Notably, changes in directionality (i.e., higher proportion of anterogradely traveling LDCVs) were observed only in dendrites, and only in response to SL. Finally, changes in VP-LDCV trafficking dynamics in response to chronic osmotic stimulation were much more pronounced compared to acute increases in VP activity/release (e.g., a max speed increase of 25% after acute NMDA versus 96% and 131% increase in WD or SL, respectively, compared to baseline). The molecular mechanisms by which an increased hormonal demand can result in changes in VP-LDCV trafficking dynamics are at present unknown. Work from different laboratories over the past decades has clearly demonstrated that systemic VP release is dependent on the degree and pattern of firing activity of these neurons,[9–11] both of which are also dependent on the osmotic state of the animal.[73,74] Moreover, abundant data support a high degree of activity and release of VP both in water-deprived and salt-loaded rats.[43,44,75,76] While we did not measure simultaneous LDCV dynamics and VP release, based on the wealth of previous studies we can confidently state that the increased velocity of LDCV under sustained osmotic stimulation correlates with an increased activity and release of VP in the system.

Additionally, a recent study showed that microtubule density is upregulated in VP neurons after SL, supporting a contribution of microtubules to the osmotic response.[77] This restructuring and expansion of the microtubule network could provide further avenues for active transport, accounting, at least in part, for the upregulated LDCV transport kinetics that we report in this study. Another possibility is that microtubule-mediated transport is known to be regulated through post-translational modifications of tubulins or motor proteins.[52,78–82] This could reflect the presence of several post-translational modifications to microtubules, allowing for a wide variety of active transport properties, functions, and destinies for trafficked LDCVs.[81,82] Still, whether this mechanism contributes to upregulating VP-LDCV trafficking during osmotic challenges remains to be determined.

Together, these results support the notion that in response to conditions of increased hormonal demand, VP neurons upregulate LDCV trafficking both in dendrites and axons to maintain appropriate levels of readily releasable pools of neuropeptide during states of increased demands, particularly during prolonged stimulation. A large body of evidence showed that, under these challenging conditions, the magnocellular neurosecretory system experiences a phenomenal degree of structural/functional plasticity, including adoption of specific firing patterns,[74,83,84] changes in the neuronal-glial-vascular microenvironment,[38,57,85] and transcriptomic changes as well,[46,86] all of which are necessary for the optimal facilitation of hormone release and reestablishment of fluid/electrolyte homeostasis. Results from the present study suggest that adaptive changes in LDCV trafficking dynamics constitute another important factor contributing to the overall VP adaptive responses to cope with systemic challenges to homeostasis.

Limitations of the study

Only male subjects were used in this study; thus, the influence of sex on the results of the study cannot be determined. Furthermore, this study was performed using an acute slice preparation of the neurons. Trafficking properties observed in this preparation may not reflect kinetics as they exist *in vivo*.

STAR★METHODS

Detailed methods are provided in the online version of this paper and include the following:

- KEY RESOURCES TABLE
- RESOURCE AVAILABILITY
  - Lead contact
  - Materials availability
  - Data and code availability
- EXPERIMENTAL MODEL AND STUDY PARTICIPANT DETAILS
- METHODS DETAILS
  - Acute slice preparation
  - 2 photon microscopy
- QUANTIFICATION AND STATISTICAL ANALYSIS

SUPPLEMENTAL INFORMATION

Supplemental information can be found online at https://doi.org/10.1016/j.isci.2023.108243.

ACKNOWLEDGMENTS

Funding: NIH K99HL168434 (M.K.K.), DFG AL 2466/2-1 (F.A.), R01 NS115209 (D.N.C.), R01 NINDS 094640 and R01 HL162575-01 (J.E.S). K.D. is supported by 2CI Neurogenomics Fellowship (GSU), a Brains & Behavior Fellowship (GSU), and a Kenneth W. and Georganne F. Honeycutt Fellowship (GSU).

AUTHOR CONTRIBUTIONS

Conceptualization, J.E.S. and M.K.K.; Methodology, J.E.S., M.K.K., and F.A.; Formal Analysis, M.K.K. and K.D.; Investigation, M.K.K. and F.A.; Resources, J.E.S.; Writing – Original Draft, J.E.S. and M.K.K.; Writing – Review & Editing, J.E.S., M.K.K., F.A., K.D., and D.N.C.; Visualization, M.K.K. and K.D.; Supervision, J.E.S. and D.N.C.; Project Administration, J.E.S.; Funding Acquisition, M.K.K. and J.E.S.

DECLARATION OF INTERESTS

The authors declare no competing interests.

Received: May 31, 2023
Revised: August 28, 2023
Accepted: October 16, 2023
Published: October 18, 2023

REFERENCES

1. Guedes-Dias, P., and Holzbaur, E.L.F. (2019). Axonal transport: Driving synaptic function. Science *366*, eaaw9997. https://doi.org/10.1126/science.aaw9997.
2. Liu, Y., Shuai, K., Sun, Y., Zhu, L., and Wu, X.-M. (2022). Advances in the study of axon–associated vesicles. Front. Mol. Neurosci. *15*.
3. Henny, P., and Jones, B.E. (2006). Vesicular glutamate (VGlut), GABA (VGAT), and acetylcholine (VACht) transporters in basal forebrain axon terminals innervating the lateral hypothalamus. J. Comp. Neurol. *496*, 453–467. https://doi.org/10.1002/cne.20928.
4. Li, C., and Kim, K. (2008). Neuropeptides. WormBook, 1–36. https://doi.org/10.1895/wormbook.1.142.1.

5. Russo, A.F. (2017). Overview of neuropeptides: awakening the senses? Headache *57*, 37–46. https://doi.org/10.1111/head.13084.
6. Moos, F., Poulain, D.A., Rodriguez, F., Guerné, Y., Vincent, J.D., and Richard, P. (1989). Release of oxytocin within the supraoptic nucleus during the milk ejection reflex in rats. Exp. Brain Res. *76*, 593–602. https://doi.org/10.1007/BF00248916.
7. Stricker, E.M., Hosutt, J.A., and Verbalis, J.G. (1987). Neurohypophyseal secretion in hypovolemic rats: inverse relation to sodium appetite. Am. J. Physiol. *252*, R889–R896. https://doi.org/10.1152/ajpregu.1987.252.5.R889.
8. Leng, G., Brown, C.H., and Russell, J.A. (1999). Physiological pathways regulating the activity of magnocellular neurosecretory cells. Prog. Neurobiol. *57*, 625–655. https://doi.org/10.1016/S0301-0082(98)00072-0.
9. Dutton, A., and Dyball, R.E. (1979). Phasic firing enhances vasopressin release from the rat neurohypophysis. J. Physiol. *290*, 433–440.
10. Bicknell, R.J., and Leng, G. (1981). Relative efficiency of neural firing patterns for vasopressin release in vitro. Neuroendocrinology *33*, 295–299.
11. Cazalis, M., Dayanithi, G., and Nordmann, J.J. (1985). The role of patterned burst and interburst interval on the excitation-coupling mechanism in the isolated rat neural lobe. J. Physiol. *369*, 45–60.
12. Armstrong, W.E. (2007). The neurophysiology of neurosecretory cells. J. Physiol. *585*, 645–647. https://doi.org/10.1113/jphysiol.2007.145755.
13. Ludwig, M. (1998). Dendritic release of vasopressin and oxytocin. J. Neuroendocrinol. *10*, 881–895.
14. Ludwig, M., and Leng, G. (2006). Dendritic peptide release and peptide-dependent behaviours. Nat. Rev. Neurosci. *7*, 126–136. https://doi.org/10.1038/nrn1845.
15. Brown, C.H., Ludwig, M., Tasker, J.G., and Stern, J.E. (2020). Somato-dendritic vasopressin and oxytocin secretion in endocrine and autonomic regulation. J. Neuroendocrinol. *32*, e12856. https://doi.org/10.1111/jne.12856.
16. Pow, D.V., and Morris, J.F. (1989). Dendrites of hypothalamic magnocellular neurons release neurohypophysial peptides by exocytosis. Neuroscience *32*, 435–439.
17. Ludwig, M., Sabatier, N., Bull, P.M., Landgraf, R., Dayanithi, G., and Leng, G. (2002). Intracellular calcium stores regulate activity-dependent neuropeptide release from dendrites. Nature *418*, 85–89. https://doi.org/10.1038/nature00822.
18. Tobin, V.A., Douglas, A.J., Leng, G., and Ludwig, M. (2011). The Involvement of Voltage-Operated Calcium Channels in Somato-Dendritic Oxytocin Release. PLoS One *6*, e25366. https://doi.org/10.1371/journal.pone.0025366.
19. Son, S.J., Filosa, J.A., Potapenko, E.S., Biancardi, V.C., Zheng, H., Patel, K.P., Tobin, V.A., Ludwig, M., and Stern, J.E. (2013). Dendritic Peptide Release Mediates Interpopulation Crosstalk between Neurosecretory and Preautonomic Networks. Neuron *78*, 1036–1049. https://doi.org/10.1016/j.neuron.2013.04.025.
20. Hurbin, A., Orcel, H., Alonso, G., Moos, F., and Rabié, A. (2002). The vasopressin receptors colocalize with vasopressin in the magnocellular neurons of the rat supraoptic nucleus and are modulated by water balance. Endocrinology *143*, 456–466. https://doi.org/10.1210/endo.143.2.8643.
21. Sabatier, N., Richard, P., and Dayanithi, G. (1998). Activation of multiple intracellular transduction signals by vasopressin in vasopressin-sensitive neurones of the rat supraoptic nucleus. J. Physiol. *513*, 699–710. https://doi.org/10.1111/j.1469-7793.1998.699ba.x.
22. Tobin, V.A., Hurst, G., Norrie, L., Dal Rio, F.P., Bull, P.M., and Ludwig, M. (2004). Thapsigargin-induced mobilization of dendritic dense-cored vesicles in rat supraoptic neurons. Eur. J. Neurosci. *19*, 2909–2912. https://doi.org/10.1111/j.1460-9568.2004.03388.x.
23. Sabatier, N., Caquineau, C., Dayanithi, G., Bull, P., Douglas, A.J., Guan, X.M.M., Jiang, M., Van der Ploeg, L., and Leng, G. (2003). Alpha-melanocyte-stimulating hormone stimulates oxytocin release from the dendrites of hypothalamic neurons while inhibiting oxytocin release from their terminals in the neurohypophysis. J. Neurosci. *23*, 10351–10358. https://doi.org/10.1523/JNEUROSCI.23-32-10351.2003.
24. Pitra, S., Zhang, M., Cauley, E., and Stern, J.E. (2019). NMDA receptors potentiate activity-dependent dendritic release of neuropeptides from hypothalamic neurons. J. Physiol. *597*, 1735–1756. https://doi.org/10.1113/JP277167.
25. Lemos, J.R., Ortiz-Miranda, S.I., Cuadra, A.E., Velázquez-Marrero, C., Custer, E.E., Dad, T., and Dayanithi, G. (2012). Modulation/physiology of calcium channel sub-types in neurosecretory terminals. Cell Calcium *51*, 284–292. https://doi.org/10.1016/j.ceca.2012.01.008.
26. Leng, G., and Ludwig, M. (2008). Neurotransmitters and peptides: whispered secrets and public announcements. J. Physiol. *586*, 5625–5632. https://doi.org/10.1113/jphysiol.2008.159103.
27. Brown, C.H. (2016). Magnocellular Neurons and Posterior Pituitary Function. Compr. Physiol. *6*, 1701–1741. https://doi.org/10.1002/cphy.c150053.
28. Laurent, P., Ch'ng, Q., Jospin, M., Chen, C., Lorenzo, R., and de Bono, M. (2018). Genetic dissection of neuropeptide cell biology at high and low activity in a defined sensory neuron. Proc. Natl. Acad. Sci. USA *115*, E6890–E6899. https://doi.org/10.1073/pnas.1714610115.
29. Kim, T., Gondré-Lewis, M.C., Arnaoutova, I., and Loh, Y.P. (2006). Dense-core secretory granule biogenesis. Physiology *21*, 124–133. https://doi.org/10.1152/physiol.00043.2005.
30. Ueta, Y., Fujihara, H., Serino, R., Dayanithi, G., Ozawa, H., Matsuda, K.i., Kawata, M., Yamada, J., Ueno, S., Fukuda, A., and Murphy, D. (2005). Transgenic expression of enhanced green fluorescent protein enables direct visualization for physiological studies of vasopressin neurons and isolated nerve terminals of the rat. Endocrinology *146*, 406–413. https://doi.org/10.1210/en.2004-0830.
31. Nissen, R., Hu, B., and Renaud, L.P. (1995). Regulation of spontaneous phasic firing of rat supraoptic vasopressin neurones in vivo by glutamate receptors. J. Physiol. *484*, 415–424.
32. Oliet, S.H., and Bourque, C.W. (1992). Properties of supraoptic magnocellular neurones isolated from the adult rat. J. Physiol. *455*, 291–306.
33. Oliet, S.H., and Bourque, C.W. (1993). Mechanosensitive channels transduce osmosensitivity in supraoptic neurons. Nature *364*, 341–343. https://doi.org/10.1038/364341a0.
34. Kusano, K., House, S.B., and Gainer, H. (1999). Effects of Osmotic Pressure and Brain-Derived Neurotrophic Factor on the Survival of Postnatal Hypothalamic Oxytocinergic and Vasopressinergic Neurons in Dissociated Cell Culture. J. Neuroendocrinol. *11*, 145–152. https://doi.org/10.1046/j.1365-2826.1999.00296.x.
35. Leng, G., Brown, C.H., Bull, P.M., Brown, D., Scullion, S., Currie, J., Blackburn-Munro, R.E., Feng, J., Onaka, T., Verbalis, J.G., et al. (2001). Responses of magnocellular neurons to osmotic stimulation involves coactivation of excitatory and inhibitory input: an experimental and theoretical analysis. J. Neurosci. *21*, 6967–6977. https://doi.org/10.1523/JNEUROSCI.21-17-06967.2001.
36. Kawasaki, M., Yamaguchi, K., Saito, J., Ozaki, Y., Mera, T., Hashimoto, H., Fujihara, H., Okimoto, N., Ohnishi, H., Nakamura, T., and Ueta, Y. (2005). Expression of immediate early genes and vasopressin heteronuclear RNA in the paraventricular and supraoptic nuclei of rats after acute osmotic stimulus. J. Neuroendocrinol. *17*, 227–237. https://doi.org/10.1111/j.1365-2826.2005.01297.x.
37. Fujio, T., Fujihara, H., Shibata, M., Yamada, S., Onaka, T., Tanaka, K., Morita, H., Dayanithi, G., Kawata, M., Murphy, D., and Ueta, Y. (2006). Exaggerated Response of Arginine Vasopressin-Enhanced Green Fluorescent Protein Fusion Gene to Salt Loading without Disturbance of Body Fluid Homeostasis in Rats. J. Neuroendocrinol. *18*, 776–785. https://doi.org/10.1111/j.1365-2826.2006.01476.x.
38. Roy, R.K., Althammer, F., Seymour, A.J., Du, W., Biancardi, V.C., Hamm, J.P., Filosa, J.A., Brown, C.H., and Stern, J.E. (2021). Inverse neurovascular coupling contributes to positive feedback excitation of vasopressin neurons during a systemic homeostatic challenge. Cell Rep. *37*, 109925. https://doi.org/10.1016/j.celrep.2021.109925.
39. Neupane, C., Sharma, R., Pai, Y.H., Lee, S.Y., Jeon, B.H., Kim, H.-W., Stern, J.E., and Park, J.B. (2021). High Salt Intake Recruits Tonic Activation of NR2D Subunit-Containing Extrasynaptic NMDARs in Vasopressin Neurons. J. Neurosci. *41*, 1145–1156. https://doi.org/10.1523/JNEUROSCI.1742-20.2020.
40. Satoh, K., Oti, T., Katoh, A., Ueta, Y., Morris, J.F., Sakamoto, T., and Sakamoto, H. (2015). In vivo processing and release into the circulation of GFP fusion protein in arginine vasopressin enhanced GFP transgenic rats: response to osmotic stimulation. FEBS J. *282*, 2488–2499. https://doi.org/10.1111/febs.13291.
41. Antunes-Rodrigues, J., Ruginsk, S.G., Mecawi, A.S., Margatho, L.O., Reis, W.L., Ventura, R.R., da Silva, A.L., Vilhena-Franco, T., and Elias, L.L.K. (2014). Neuroendocrinology of Hydromineral Homeostasis. In Neurobiology of Body Fluid Homeostasis: Transduction and Integration Frontiers in Neuroscience, L.A. De Luca, J.V. Menani, and A.K. Johnson, eds. (CRC Press/Taylor & Francis).

42. Di, S., Jiang, Z., Wang, S., Harrison, L.M., Castro-Echeverry, E., Stuart, T.C., Wolf, M.E., and Tasker, J.G. (2019). Labile Calcium-Permeable AMPA Receptors Constitute New Glutamate Synapses Formed in Hypothalamic Neuroendocrine Cells during Salt Loading. eNeuro *6*, ENEURO.0112-0119.2019. https://doi.org/10.1523/ENEURO.0112-19.2019.
43. Levi, D.I., Wyrosdic, J.C., Hicks, A.-I., Andrade, M.A., Toney, G.M., Prager-Khoutorsky, M., and Bourque, C.W. (2021). High dietary salt amplifies osmoresponsiveness in vasopressin-releasing neurons. Cell Rep. *34*, 108866. https://doi.org/10.1016/j.celrep.2021.108866.
44. Morita, M., Kita, Y., and Notsu, Y. (2001). Mechanism of AVP release and synthesis in chronic salt-loaded rats. J. Pharm. Pharmacol. *53*, 1703–1709. https://doi.org/10.1211/0022357011778106.
45. Yoshimura, M., Ohkubo, J., Katoh, A., Ohno, M., Ishikura, T., Kakuma, T., Yoshimatsu, H., Murphy, D., and Ueta, Y. (2013). A c-fos-monomeric red fluorescent protein 1 fusion transgene is differentially expressed in rat forebrain and brainstem after chronic dehydration and rehydration. J. Neuroendocrinol. *25*, 478–487. https://doi.org/10.1111/jne.12022.
46. Greenwood, M.P., Mecawi, A.S., Hoe, S.Z., Mustafa, M.R., Johnson, K.R., Al-Mahmoud, G.A., Elias, L.L.K., Paton, J.F.R., Antunes-Rodrigues, J., Gainer, H., et al. (2015). A comparison of physiological and transcriptome responses to water deprivation and salt loading in the rat supraoptic nucleus. Am. J. Physiol. Regul. Integr. Comp. Physiol. *308*, R559–R568. https://doi.org/10.1152/ajpregu.00444.2014.
47. da Silveira, L.T.G., Junta, C.M., Monesi, N., de Oliveira-Pelegrin, G.R., Passos, G.A., and Rocha, M.J.A. (2007). Time course of c-fos, vasopressin and oxytocin mRNA expression in the hypothalamus following long-term dehydration. Cell. Mol. Neurobiol. *27*, 575–584. https://doi.org/10.1007/s10571-007-9144-2.
48. de Wit, J., Toonen, R.F., Verhaagen, J., and Verhage, M. (2006). Vesicular trafficking of semaphorin 3A is activity-dependent and differs between axons and dendrites. Traffic *7*, 1060–1077. https://doi.org/10.1111/j.1600-0854.2006.00442.x.
49. Park, J.J., Cawley, N.X., and Loh, Y.P. (2008). A bi-directional carboxypeptidase E-driven transport mechanism controls BDNF vesicle homeostasis in hippocampal neurons. Mol. Cell. Neurosci. *39*, 63–73. https://doi.org/10.1016/j.mcn.2008.05.016.
50. de Jong, E.K., Vinet, J., Stanulovic, V.S., Meijer, M., Wesseling, E., Sjollema, K., Boddeke, H.W.G.M., and Biber, K. (2008). Expression, transport, and axonal sorting of neuronal CCL21 in large dense-core vesicles. Faseb. J. *22*, 4136–4145. https://doi.org/10.1096/fj.07-101907.
51. Wong, M.Y., Zhou, C., Shakiryanova, D., Lloyd, T.E., Deitcher, D.L., and Levitan, E.S. (2012). Neuropeptide delivery to synapses by long-range vesicle circulation and sporadic capture. Cell *148*, 1029–1038. https://doi.org/10.1016/j.cell.2011.12.036.
52. Knabbe, J., Nassal, J.P., Verhage, M., and Kuner, T. (2018). Secretory vesicle trafficking in awake and anaesthetized mice: differential speeds in axons versus synapses. J. Physiol. *596*, 3759–3773. https://doi.org/10.1113/JP276022.
53. Rolls, M.M. (2022). Principles of microtubule polarity in linear cells. Dev. Biol. *483*, 112–117. https://doi.org/10.1016/j.ydbio.2022.01.004.
54. Bittins, C.M., Eichler, T.W., Hammer, J.A., and Gerdes, H.-H. (2010). Dominant-negative myosin Va impairs retrograde but not anterograde axonal transport of large dense core vesicles. Cell. Mol. Neurobiol. *30*, 369–379. https://doi.org/10.1007/s10571-009-9459-2.
55. Kwinter, D.M., Lo, K., Mafi, P., and Silverman, M.A. (2009). Dynactin regulates bidirectional transport of dense-core vesicles in the axon and dendrites of cultured hippocampal neurons. Neuroscience *162*, 1001–1010. https://doi.org/10.1016/j.neuroscience.2009.05.038.
56. Stern, J.E., Hestrin, S., and Armstrong, W.E. (2000). Enhanced neurotransmitter release at glutamatergic synapses on oxytocin neurones during lactation in the rat. J. Physiol. (Lond.) *526*, 109–114.
57. Oliet, S.H., Piet, R., and Poulain, D.A. (2001). Control of glutamate clearance and synaptic efficacy by glial coverage of neurons. Science *292*, 923–926. https://doi.org/10.1126/science.1059162.
58. Teruyama, R., Lipschitz, D.L., Wang, L., Ramoz, G.R., Crowley, W.R., Bealer, S.L., and Armstrong, W.E. (2008). Central blockade of oxytocin receptors during mid-late gestation reduces amplitude of slow afterhyperpolarization in supraoptic oxytocin neurons. Am. J. Physiol. Endocrinol. Metab. *295*, E1167–E1171. https://doi.org/10.1152/ajpendo.90620.2008.
59. Choe, K.Y., Han, S.Y., Gaub, P., Shell, B., Voisin, D.L., Knapp, B.A., Barker, P.A., Brown, C.H., Cunningham, J.T., and Bourque, C.W. (2015). High Salt Intake Increases Blood Pressure via BDNF-Mediated Downregulation of KCC2 and Impaired Baroreflex Inhibition of Vasopressin Neurons. Neuron *85*, 549–560. https://doi.org/10.1016/j.neuron.2014.12.048.
60. Potapenko, E.S., Biancardi, V.C., Zhou, Y., and Stern, J.E. (2012). Altered astrocyte glutamate transporter regulation of hypothalamic neurosecretory neurons in heart failure rats. Am. J. Physiol. Regul. Integr. Comp. Physiol. *303*, R291–R300. https://doi.org/10.1152/ajpregu.00056.2012.
61. Fleming, T.M., Scott, V., Naskar, K., Joe, N., Brown, C.H., and Stern, J.E. (2011). State-dependent changes in astrocyte regulation of extrasynaptic NMDA receptor signalling in neurosecretory neurons. J. Physiol. *589*, 3929–3941. https://doi.org/10.1113/jphysiol.2011.207340.
62. Grimaud, B., Frétaud, M., Terras, F., Bénassy, A., Duroure, K., Bercier, V., Trippé-Allard, G., Mohammedi, R., Gacoin, T., Del Bene, F., et al. (2022). In Vivo Fast Nonlinear Microscopy Reveals Impairment of Fast Axonal Transport Induced by Molecular Motor Imbalances in the Brain of Zebrafish Larvae. ACS Nano *16*, 20470–20487. https://doi.org/10.1021/acsnano.2c06799.
63. Persoon, C.M., Moro, A., Nassal, J.P., Farina, M., Broeke, J.H., Arora, S., Dominguez, N., van Weering, J.R., Toonen, R.F., and Verhage, M. (2018). Pool size estimations for dense-core vesicles in mammalian CNS neurons. EMBO J. *37*, e99672. https://doi.org/10.15252/embj.201899672.
64. Nordmann, J.J., and Morris, J.F. (1984). Method for quantitating the molecular content of a subcellular organelle: hormone and neurophysin content of newly formed and aged neurosecretory granules. Proc. Natl. Acad. Sci. USA *81*, 180–184. https://doi.org/10.1073/pnas.81.1.180.
65. Borges-Merjane, C., Kim, O., and Jonas, P. (2020). Functional Electron Microscopy, "Flash and Freeze," of Identified Cortical Synapses in Acute Brain Slices. Neuron *105*, 992–1006.e6. https://doi.org/10.1016/j.neuron.2019.12.022.
66. Ludwig, M., Bull, P.M., Tobin, V.A., Sabatier, N., Landgraf, R., Dayanithi, G., and Leng, G. (2005). Regulation of activity-dependent dendritic vasopressin release from rat supraoptic neurones. J. Physiol. *564*, 515–522. https://doi.org/10.1113/jphysiol.2005.083931.
67. Xiong, J.-J., and Hatton, G.I. (1996). Differential responses of oxytocin and vasopressin neurons to the osmotic and stressful components of hypertonic saline injections: a Fos protein double labeling study. Brain Res. *719*, 143–153. https://doi.org/10.1016/0006-8993(95)01466-7.
68. Ludwig, M., Horn, T., Callahan, M.F., Grosche, A., Morris, M., and Landgraf, R. (1994). Osmotic stimulation of the supraoptic nucleus: central and peripheral vasopressin release and blood pressure. Am. J. Physiol. *266*, E351–E356. https://doi.org/10.1152/ajpendo.1994.266.3.E351.
69. Ludwig, M., Callahan, M.F., Neumann, I., Landgraf, R., and Morris, M. (1994). Systemic osmotic stimulation increases vasopressin and oxytocin release within the supraoptic nucleus. J. Neuroendocrinol. *6*, 369–373. https://doi.org/10.1111/j.1365-2826.1994.tb00595.x.
70. Ludwig, M., Williams, K., Callahan, M.F., and Morris, M. (1996). Salt loading abolishes osmotically stimulated vasopressin release within the supraoptic nucleus. Neurosci. Lett. *215*, 1–4. https://doi.org/10.1016/s0304-3940(96)12956-6.
71. Tweedle, C.D., and Hatton, G.I. (1976). Ultrastructural comparisons of neurons of supraoptic and circularis nuclei in normal and dehydrated rats. Brain Res. Bull. *1*, 103–121. https://doi.org/10.1016/0361-9230(76)90054-X.
72. Wakerley, J.B., Poulain, D.A., and Brown, D. (1978). Comparison of firing patterns in oxytocin- and vasopressin-releasing neurones during progressive dehydration. Brain Res. *148*, 425–440. https://doi.org/10.1016/0006-8993(78)90730-8.
73. Summy-Long, J.Y., and Kadekaro, M. (2001). Role of circumventricular organs (CVO) in neuroendocrine responses: interactions of CVO and the magnocellular neuroendocrine system in different reproductive states. Clin. Exp. Pharmacol. Physiol. *28*, 590–601. https://doi.org/10.1046/j.1440-1681.2001.03491.x.
74. Bourque, C.W., and Renaud, L.P. (1984). Activity patterns and osmosensitivity of rat supraoptic neurones in perfused hypothalamic explants. J. Physiol. *349*, 631–642.
75. Keil, L.C., Barbella, Y.R., Dundore, R.L., Wurpel, J.N., and Severs, W.B. (1983). Vasopressin release induced by water deprivation: effects of centrally

administered saralasin. Neuroendocrinology *37*, 401–405. https://doi.org/10.1159/000123583.
76. Thornton, S.N., Leng, G., Bicknell, R.J., Chapman, C., and Purdew, T. (1986). Vasopressin, but not oxytocin, is released in response to water deprivation in conscious goats. J. Endocrinol. *110*, 335–340. https://doi.org/10.1677/joe.0.1100335.
77. Hicks, A.-I., Barad, Z., Sobrero, A., Lean, G., Jacob-Tomas, S., Yang, J., Choe, K.Y., and Prager-Khoutorsky, M. (2020). Effects of salt loading on the organisation of microtubules in rat magnocellular vasopressin neurones. J. Neuroendocrinol. *32*, e12817. https://doi.org/10.1111/jne.12817.
78. Schlager, M.A., and Hoogenraad, C.C. (2009). Basic mechanisms for recognition and transport of synaptic cargos. Mol. Brain *2*, 25. https://doi.org/10.1186/1756-6606-2-25.
79. Akhmanova, A., and Hammer, J.A. (2010). Linking molecular motors to membrane cargo. Curr. Opin. Cell Biol. *22*, 479–487. https://doi.org/10.1016/j.ceb.2010.04.008.
80. Hirokawa, N., Niwa, S., and Tanaka, Y. (2010). Molecular motors in neurons: transport mechanisms and roles in brain function, development, and disease. Neuron *68*, 610–638. https://doi.org/10.1016/j.neuron.2010.09.039.
81. Janke, C., and Chloë Bulinski, J. (2011). Post-translational regulation of the microtubule cytoskeleton: mechanisms and functions. Nat. Rev. Mol. Cell Biol. *12*, 773–786. https://doi.org/10.1038/nrm3227.
82. Sirajuddin, M., Rice, L.M., and Vale, R.D. (2014). Regulation of microtubule motors by tubulin isotypes and post-translational modifications. Nat. Cell Biol. *16*, 335–344. https://doi.org/10.1038/ncb2920.
83. Brimble, M.J., and Dyball, R.E. (1977). Characterization of the responses of oxytocin- and vasopressin-secreting neurones in the supraoptic nucleus to osmotic stimulation. J. Physiol. *271*, 253–271.
84. Stern, J.E., and Armstrong, W.E. (1996). Changes in the Electrical Properties of Supraoptic Nucleus Oxytocin and Vasopressin Neurons during Lactation. J. Neurosci. *16*, 4861–4871.
85. Du, W., Stern, J.E., and Filosa, J.A. (2015). Neuronal-Derived Nitric Oxide and Somatodendritically Released Vasopressin Regulate Neurovascular Coupling in the Rat Hypothalamic Supraoptic Nucleus. J. Neurosci. *35*, 5330–5341. https://doi.org/10.1523/JNEUROSCI.3674-14.2015.
86. Chen, S., Xu, H., Dong, S., and Xiao, L. (2022). Morpho-Electric Properties and Diversity of Oxytocin Neurons in Paraventricular Nucleus of Hypothalamus in Female and Male Mice. J. Neurosci. *42*, 2885–2904. https://doi.org/10.1523/JNEUROSCI.2494-21.2022.
87. Aghajanian, G.K., and Rasmussen, K. (1989). Intracellular studies in the facial nucleus illustrating a simple new method for obtaining viable motoneurons in adult rat brain slices. Synapse *3*, 331–338. https://doi.org/10.1002/syn.890030406.
88. B. Sakmann, and E. Neher, eds. (1995). Single-Channel Recording (Springer US). https://doi.org/10.1007/978-1-4419-1229-9.
89. Armstrong, W.E., Schöler, J., and McNeill, T.H. (1982). Immunocytochemical, Golgi and electron microscopic characterization of putative dendrites in the ventral glial lamina of the rat supraoptic nucleus. Neuroscience *7*, 679–694. https://doi.org/10.1016/0306-4522(82)90074-4.
90. Armstrong, W.E. (1995). Morphological and electrophysiological classification of hypothalamic supraoptic neurons. Prog. Neurobiol. *47*, 291–339. https://doi.org/10.1016/0301-0082(95)80005-S.
91. Smith, B.N., and Armstrong, W.E. (1990). Tuberal supraoptic neurons—I. Morphological and electrophysiological characteristics observed with intracellular recording and biocytin filling in vitro. Neuroscience *38*, 469–483. https://doi.org/10.1016/0306-4522(90)90043-4.
92. Randle, J.C., Bourque, C.W., and Renaud, L.P. (1986). Serial reconstruction of lucifer yellow-labeled supraoptic nucleus neurons in perfused rat hypothalamic explants. Neuroscience *17*, 453–467. https://doi.org/10.1016/0306-4522(86)90259-9.
93. Lefranc, G. (1966). [Neurohistologic study of the supraoptic and paraventricular nuclei in guinea pigs and cats by the Golgi triple impregnation technic]. C. R. Acad. Hebd. Seances Acad. Sci. D. *263*, 976–979.
94. Stern, J.E. (2001). Electrophysiological and morphological properties of pre-autonomic neurones in the rat hypothalamic paraventricular nucleus. J. Physiol. (Lond.) *537*, 161–177. https://doi.org/10.1111/j.1469-7793.2001.0161k.x.
95. Tasker, J.G., and Dudek, F.E. (1991). Electrophysiological properties of neurones in the region of the paraventricular nucleus in slices of rat hypothalamus. J. Physiol. *434*, 271–293.
96. Luther, J.A., Daftary, S.S., Boudaba, C., Gould, G.C., Halmos, K.C., and Tasker, J.G. (2002). Neurosecretory and non-neurosecretory parvocellular neurones of the hypothalamic paraventricular nucleus express distinct electrophysiological properties. J. Neuroendocrinol. *14*, 929–932.
97. Sofroniew, M.V. (1985). Vasopressin- and neurophysin-immunoreactive neurons in the septal region, medial amygdala and locus coeruleus in colchicine-treated rats. Neuroscience *15*, 347–358. https://doi.org/10.1016/0306-4522(85)90217-9.
98. Swanson, L.W., and Sawchenko, P.E. (1983). Hypothalamic integration: organization of the paraventricular and supraoptic nuclei. Annu. Rev. Neurosci. *6*, 269–324. https://doi.org/10.1146/annurev.ne.06.030183.001413.
99. R Core Team (2021). R: A Language and Environment for Statistical Computing.
100. Wickham, H. (2016). ggplot2: Elegant Graphics for Data Analysis (Springer Science & Business Media).

STAR★METHODS

KEY RESOURCES TABLE

REAGENT or RESOURCE	SOURCE	IDENTIFIER
Chemicals, peptides, and recombinant proteins		
Tetrodotoxin (TTX)	Alomone Labs	Cat#T-550
Mannitol	Sigma-Alderich	Cat#M9647
N-methyl-D-aspartic acid (NMDA)	Sigma-Alderich	Cat#M3262
Experimental models: Organisms/strains		
Rattus norvegicus: eGFP-VP	Ueta et al.[30]	N/A
Software and algorithms		
Imaris	Bitplane Imaris/Oxford Instruments	RRID:SCR_007370
GraphPad Prism	GraphPad Software Inc.	RRID:SCR_002798
ggplot2	R-plot	RRID:SCR_014601

RESOURCE AVAILABILITY

Lead contact

Further information and requests for resources and reagents should be directed to and will be fulfilled by the lead contact, Javier E. Stern (jstern@gsu.edu).

Materials availability

This study did not generate new unique reagents.

Data and code availability

- All data reported in this paper will be shared by the lead contact upon request.
- This paper does not report original code.
- Any additional information required to reanalyze the data reported in this paper is available from the lead contact upon request.

EXPERIMENTAL MODEL AND STUDY PARTICIPANT DETAILS

All studies described herein were approved by the Georgia State University Institutional Animal Care and Use Committee (IACUC) and align with values and guidelines for animal research outlined by the American Veterinary Medical Association.

Young adult (150-300g) transgenic male Wistar rats containing eGFP-VP were used for all experiments, and randomly assigned to each experimental group.[30] These animals received *ad libitum* food and water and were housed on a standard 12:12 light cycle. For water deprivation experiments, water bottles were removed from cages 48 h prior to experiments. For salt-loading experiments, standard drinking water was replaced with water containing 1% NaCl for seven days before experiment.

METHODS DETAILS

Acute slice preparation

On the day of the experiment, the GFP rats were anesthetized (Euthasol, Virbac, ANADA #200-071, Fort Worth, TX, USA, 50 mg kg^{-1} i.p.) and then perfused transcardially with 30 mL of ice-cold sucrose artificial cerebrospinal fluid (ACSF) (NaCl replaced by equal-osmol sucrose)[87] containing the following (in mM): 210 sucrose, 2.5 KCl, 1 $MgSO_4$, 26 $NaHCO_3$, 1.25 NaH_2PO_4, 20 D-Glucose, 0.4 ascorbic acid, and 2.0 $CaCl_2$; pH 7.2; 300–305 mosmol l^{-1}. Rats were then rapidly decapitated, and brains were subsequently dissected, mounted in the chamber of a vibrotome (Leica VT1200s, Leica Microsystems, Buffalo Grove, IL, USA), and submerged in the same sucrose solution and bubbled constantly with 95% O_2/5% CO_2 gas. Coronal slices containing the hypothalamic SON and PVN were cut at 240 μm thickness and placed in a holding chamber containing ACSF bubbled with 95% O_2/5% CO_2. The ACSF is identical in composition to the sucrose solution, but with 210 mM sucrose replaced by 119 mM NaCl and 2 mM Na^+-Pyruvate. Slices rested for a minimum of 45 min in total before any experiment.

2 photon microscopy

Slices were placed on the stage of an Olympus BX51WI upright microscope (Bruker, Billerica, MA, USA). The stage was perfused (~2 mL/min) with ACSF bubbled continuously with 95% O2/5% CO_2 and warmed to 32°C. eGFP-VP neurons were excited with a 2 photon (2P) MaiTai Laser

(Spectra-Physics, Milpitas, CA, USA) tuned to 860 nm in and imaged with a 60x Nikon LUMPLFLN60×W objective. Slices were scanned for quality processes (either an axon or dendrite) that displayed LDCV movement suitable for imaging. When imaging PVN, we targeted exclusively magnocellular VP neurons by avoiding eGFP-positive neurons with small somas, thus trafficking in parvocellular VP neurons was not evaluated. Desirable characteristics included healthy, viable eGFP-positive neurons (as assessed by characteristic morphology under DIC illumination[88]), located at least two cell layers below the surface of the slice, with processes containing moving LDCVs, low process background fluorescence, and processes that were straight and remain in the same z-plane (i.e., processes that aren't tortuous). Conversely, cells at the surface of the slice often displayed inert LDCV movement along with visual characteristic of damaged cells under DIC (swollen somata, dull and loosely defined edges, visible nucleus).[88] Given these cells were likely damaged by the slicing procedure, we did not image them.

Some neurons had inert LDCV movement and thus we did not evaluate these neurons due to concerns about cell viability. With regards to dendrites, we exclusively imaged first order dendrites,[89–93] favoring neurons with thick apical dendrites as these tended to have lower background fluorescence and thus made analysis more accurate. We only imaged processes with a minimum of 15 μm visible in a single z-plane. All dendrite measurements labeled "proximal" refer to initial dendrite segments at the point where they join with the soma. Distal dendrite measurements are segments greater than 50 μm from the soma. Axons were identified based on their very narrow width (i.e., the same size as a single vesicle diameter) and long length (hundreds of microns). All axon measurements were imaged at least 20 μm from the soma and care was taken to ensure that any imaged process was not severed from its soma. During acquisition, we employed a 3x digital zoom and cropped the process to maximize spatiotemporal resolution. We scanned using resonant galvo mode with 16x frame averaging. Laser power, photomultiplier tube (PMT) sensitivity, field of view, and scan speed all varied between trials to maximize spatiotemporal resolution without photobleaching the specimen. Imaging acquisition occurred for 1–2 min per process. Trials in which acute pharmacological challenges were presented to the same process, imaging settings and acquisition time remained consistent before and after drug application. The goal of these studies was to measure LDCV kinetics, thus maximizing acquisition of quality time series to ensure accurate tracking was prioritized over maintaining consistent acquisition parameters across trials.

QUANTIFICATION AND STATISTICAL ANALYSIS

VP magnocellular neurosecretory neurons from both SON and PVN were evaluated. While SON contains only magnocellular type neurons, PVN contains both magnocellular and parvocellular VP neurons which have distinct morphological and electrophysiological properties.[94–97] When evaluating VP neurons from PVN, we targeted magnocellular neurons located in the lateral magnocellular subdivision, which contains the majority of VP magnocellular neurons.[98] Given the parity of magnocellular VP neurons from SON and PVN, data obtained from these VP neurons were pooled together for analysis.

Images were imported and analyzed in Imaris (Andor Technology, Belfast, Northern Ireland) for spot detection and tracking. First, images were background subtracted and a mask was created for each time series to isolate the imaged dendrite or axon and eliminate potential spot detection outside of the target. A reference point was placed in the center of the dendritic or axonal hillock so that measurements could be calculated in relation to this reference point. Next, we ran the 'spots' pipeline function to detect LDCVs and track movement. The 'spots quality' parameter was adjusted between trials to maximize accurate detection of particle movement. However, this remained the same in trials where the same process was being analyzed, such as before and after an acute pharmacological application. The following parameters remained the same: Track Spots: Yes, Estimated XY Diameter: 0.3 μm, Background Subtraction: Yes, Algorithm: Autoregressive Motion, Max Distance: 0.4, Max Gap Size: 1. Only LDCVs that could be observed for a minimum of 10 s and displaced a minimum of 2 μm in distance were included for analysis. Tracks were checked manually for accuracy. All data was exported as.csv files for further statistical analysis in MATLAB and PRISM. Mean and max speed were determined from the files. Directionality was calculated using the statistic "Distance from Origin Reference Frame". This parameter calculates distance of each spot from the reference point for each frame that the LDCV is tracked. The first value was subtracted from the final value. If this value was positive, the LDCV was classified as anterograde movement; if this value was negative, the LDCV was classified as retrograde movement. The positive and negative values were reassigned 1 or -1 respectively for easier analysis. Statistics and most graphics generated with GraphPad Prism (Boston, MA, USA). Error bars represent standard error of the mean (SEM) where applicable. Distribution density analyses were performed on mean speed data binned into 50 bins and subsequent kernel density plot generation was performed using R Statistical Software (v4.2.2)[99] and the ggplot2 R package (v3.3.5).[100] Table and figure n value formatting is as follows: animals | processes | LDCVs, unless otherwise noted. For anterograde vs. retrograde comparisons, only vesicle count is reported to avoid redundancy. Figure legend denotes statistical test used; asterisks in figures denote significance level (*$p < 0.05$, **$p < 0.01$, ***$p < 0.001$, ****$p < 0.0001$).